Published in final edited form as:
Stem Cells. 2013 December ; 31(12): 2620–2631. doi:10.1002/stem.1515.

Generation and characterization of spiking and non-spiking oligodendroglial progenitor cells from embryonic stem cells

Peng Jiang[1,2], **Chen Chen**[1,2], **Xiao-Bo Liu**[3], **Vimal Selvaraj**[1,2,4], **Wei Liu**[1], **Daniel H. Feldman**[2], **Ying Liu**[5], **David E. Pleasure**[2,6], **Ronald A. Li**[7], and **Wenbin Deng**[1,2,*]

[1]Department of Biochemistry and Molecular Medicine, School of Medicine, University of California, Davis, CA, USA

[2]Institute for Pediatric Regenerative Medicine, Shriners Hospitals for California, Sacramento, CA, USA

[3]Center for Neuroscience, University of California, Davis, CA, USA

[5]Department of Neurosurgery, University of Texas Health Science Center at Houston, Houston, TX, USA

[6]Departments of Neurology and Pediatrics, School of Medicine, University of California, Davis, CA, USA

[7]Departments of Medicine and Physiology, LKS Faculty of Medicine, University of Hong Kong, Hong Kong, China

Abstract

Pluripotent stem cells (PSCs) have been differentiated into oligodendroglial progenitor cells (OPCs), providing promising cell replacement therapies for many CNS disorders. Studies from rodents have shown that brain OPCs express a variety of ion channels, and that a subset of brain OPCs express voltage-gated sodium channel (Na_V), mediating the spiking properties of OPCs. However, it is unclear whether PSC-derived OPCs exhibit electrophysiological properties similar to brain OPCs and the role of Na_V in the functional maturation of OPCs is unknown. Here, using a mouse embryonic stem cell (mESC) GFP-Olig2 knockin reporter line, we demonstrated that unlike brain OPCs, all of the $GFP^+/Olig2^+$ mESC-derived OPCs (mESC-OPCs) did not express functional Na_V and failed to generate spikes (hence termed “non-spiking mESC-OPCs”), while expressing the delayed rectifier and inactivating potassium currents. By ectopically expressing

*Correspondence: Dr. Wenbin Deng, Associate Professor, UC Davis School of Medicine, Department of Biochemistry and Molecular Medicine, Institute for Pediatric Regenerative Medicine, 2425 Stockton Blvd. Sacramento, CA 95817, TEL: (916) 453-2287, FAX: (916) 453-2288, wbdeng@ucdavis.edu.
[4]Present Address: Department of Animal Science, Cornell University, NY, USA

Author Contributions

Peng Jiang, Conception and design, Collection and assembly of data, Data analysis and interpretation, Manuscript writing
Chen Chen, Collection and assembly of data, Data analysis and interpretation
Xiao-Bo Liu, Collection and assembly of data
Vimal Selvaraj, Collection and assembly of data
Wei Liu, Collection and assembly of data
Daniel H. Feldman, Collection and assembly of data
Ying Liu, Conception and design, Provision of study material
David E. Pleasure, Conception and design
Ronald A. Li, Provision of study material
Wenbin Deng, Conception and design, Financial support, Data analysis and interpretation, Manuscript writing, Final approval of manuscript

Potential Conflicts of Interest

The authors declare no conflicts of interest related to this work.

$Na_V1.2$ α subunit via viral transduction, we successfully generated mESC-OPCs with spiking properties (termed "spiking mESC-OPCs"). After transplantation into the spinal cord and brain of myelin-deficient *shiverer* mice, the spiking mESC-OPCs demonstrated better capability in differentiating into MBP expressing oligodendrocytes and in myelinating axons *in vivo* than the non-spiking mESC-OPCs. Thus, by generating spiking and non-spiking mESC-OPCs, this study reveals a novel function of Na_V in OPCs in their functional maturation and myelination, and sheds new light on ways to effectively develop PSC-derived OPCs for future clinical applications.

Keywords

Embryonic stem cell; oligodendroglial progenitor cell; voltage-gated ion channel; action potential; myelination

Introduction

Oligodendroglial progenitor cells (OPCs), also known as "NG2 glia" due to the expression of the membrane proteoglycan NG2 [1], mainly generate oligodendrocytes in the developing and mature central nervous system (CNS) [1, 2]. Electrophysiological recordings from both in situ brain slice and *in vitro* cell culture have shown that voltage-gated ion channels are expressed in rodent CNS OPCs, and that ion channel expression is developmentally regulated [3–5]. Voltage-gated potassium currents (I_K), mainly delayed rectifier potassium current (I_{KD}) and inactivating A-type potassium current (I_{KA}), are expressed in OPCs [3, 4, 6]. When OPCs mature into oligodendrocytes, another type of I_K, inward rectifier potassium current (I_{Kir}) is expressed [7]. Accumulating evidence has shown that voltage-gated sodium channel (Na_V)-mediated current (I_{Na}) is also expressed in OPCs [3–6, 8–11]. Moreover, studies have also shown that a subset of OPCs can fire action potentials upon depolarization and that this spiking property relies on the expression of Na_V [9, 10]. In oligodendrocyte lineage cells, the I_{Na} expression is specific to OPCs. When OPCs mature into oligodendrocytes, I_{Na} is not observed [3]. Despite the subdivision of spiking and non-spiking OPCs, the role of the expression of functional Na_V or in OPC development and function remains unclear.

Pluripotent stem cells (PSCs) have been successfully differentiated into OPCs [12–16] for potential regenerative therapies for oligodendrocyte injury-related CNS disorders, such as spinal cord injury [17, 18] and multiple sclerosis [19]. However, very few studies have explored the functional properties of PSC-derived OPCs, particularly their electrophysiological properties. Here, we first differentiated GFP-Olig2 mouse embryonic stem cells (mESCs), in which GFP was inserted into the Olig2 locus and thus GFP expression mirrored endogenous Olig2 expression [20], into $GFP^+/Olig2^+$ OPCs (mESC-OPCs) by the treatment of small molecules retinoic acid and purmorphamine [21, 22]. We further showed that I_{KD} and I_{KA} were expressed in GFP^+ mESC-OPCs. However, unlike in rodent CNS OPCs, the I_{Na} could not be detected in mESC-OPCs. By ectopically expressing $Na_v1.2$ α subunit, the mESC-OPCs started to express I_{Na} and acquired spiking properties. In this study, we thus refer the mESC-OPCs with and without the expression of I_{Na} as spiking and non-spiking mESC-OPCs, respectively. The generation of non-spiking mESC-OPCs and engineered spiking mESC-OPCs thus provides us with a powerful tool to explore the functional roles of I_{Na} in the OPCs. By using *in vitro* co-culture with neurons and *in vivo* transplantation into *shiverer* mice, we demonstrated that spiking mESC-OPCs had better capability of maturating into myelin basic protein (MBP) positive oligodendrocytes and myelinating axons than non-spiking mESC-OPCs. Overall, by providing the insights into the function of Na_V and engineered spiking activities in OPC maturation and myelination, this study demonstrates the need for applying ion channel physiology not only to the

differentiation of stem cells into functional glial precursor cells but also more importantly to future clinical application of stem cells.

Materials and Methods

Maintenance of mESCs

The mouse ES cell line GFP-Olig2 was obtained from the American Type Culture Collection (ATCC) and maintained using standard mESC culture methods as described in our previous studies [21, 22]. In brief, the mESCs were grown at an optimal density that required routine passaging every 3 days on irradiated MEF feeder layers (GlobalStem). The culture medium was Dulbecco's modified Eagle's medium (DMEM; GIBCO) supplemented with 20% fetal bovine serum (GIBCO), 2 mM L-glutamine (GIBCO), 1 mM sodium pyruvate (GIBCO), 0.1 mM β-mercaptoethanol (GIBCO), 0.1 mM nonessential amino acids (NEAA; GIBCO), and 1,000 U/ml leukemia inhibitory factor (Millipore).

Differentiation of mESCs

Neural differentiation of mESCs was initiated using our published protocol [21, 22]. Briefly, mESC colonies were trypsinized into single cells and suspended in differentiation medium to form embryoid bodies (EB). The differentiation medium consisted of α-minimal essential medium (α-MEM) supplemented with 20% KSR, 1 mM sodium pyruvate, 0.1mM NEAA, and 0.1 mM β-mercaptoethanol (all from GIBCO). As shown in Fig. 1A, from day 4 to day 7, retinoic acid (RA, 0.2 μM; Sigma) and purmorphamine (Pur, 1 μM; Cayman Chemical) were included in differentiation or N2 medium. The N2 medium was added from day 6 to day 7 and consisted of α-MEM supplemented with 1× N2 (GIBCO), 1 mM sodium pyruvate (GIBCO), 0.1mM NEAA, and 0.1 mM β-mercaptoethanol. At day 8, EBs were disaggregated in TrypLE (Invitrogen) and plated on poly-L-ornithine (0.002%; Sigma)/ fibronectin (10 μg/ml; Millipore) or Poly-L-ornithine (0.002%)/laminin (50 μg/ml; Sigma) coated dishes in OPC medium that consisted of Dulbecco's modified Eagle's medium with F12 (DMEM/F12; Hyclone), 1×N2, 1×B27, Pur (1μM), platelet-derived growth factor-AA (PDGF-AA, 10 ng/ml; Invitrogen) and fibroblast growth factor-2 (FGF-2, 20 ng/ml; Millipore). For further differentiation, PDGF-AA and FGF-2 was excluded from OPC medium and 3,3′5′-triido-L-thyronine (T3, 30 ng/ml; Sigma) was added to differentiate OPCs to oligodendrocytes. For testing the effects of extracellular factors on Na_V expression, heregulin (10 ng/ml; Peprotech) or laminin (5 μg/ml) were supplemented to the OPC medium.

Fluorescence-activated Cell Sorting (FACS)

We used FACS To estimate the percentage of GFP^+ cells and purify OPC populations. Single-cell suspensions were prepared the same way as during passage of mESC-OPCs [21]. Data acquisition and sorting of Olig2-GFP^+ cells were performed in a BD FACSCalibur (BD Bioscience). Acquired data were subsequently analyzed by calculating proportions/ percentages and average intensities using the FlowJo software (Treestar, Inc.).

Baculoviral Transduction

Ectopic expression of $Na_V1.2$ α subunit in mESC-OPCs was achieved by using BacMam Na^+ channel expression kit (Invitrogen). When the cells reached 70% confluency, the virus with SCN2A or control virus with GFP gene (Invitrogen) were added to the cultures according to the manufacturer's detailed protocol and our previous report [21].

Primary Culture

Highly purified mouse cortex OPCs were routinely obtained using previously published protocols [23–25]. Primary hippocampal neurons were prepared from C57BL/6 mouse fetuses (Charles River) at embryonic day 15. The hippocampi were digested with trypsin and dissociated by trituration in DMEM/F12 and 10% FBS. The hippocampal neurons were plated onto poly-D-lysine (50 μg/ml; Millipore) coated 12 mm coverslips. At day 1 in vitro (DIV 1), the medium was replaced with neuron culture medium consisted of Neurobasal medium, 1×B27 (Gibco). Cytosine arabionse (1 μM, Sigma) was added to the neurons from DIV 3 to DIV 7 to eliminate proliferating cells. At DIV 7, the non-spiking and spiking (24 h after viral infection) mESC-OPCs were plated onto the neurons at 2×10^4 cells/cm^2 in the co-culture medium consisted of 50% neuron culture medium and 50% OPC medium without FGF2 and PDGF-AA [22]. The cells were either patch-clamp recorded at 2 days after co-culture or immunostained for MBP at 10 days after co-culture.

Reverse Transcription-Polymerase Chain Reaction

Total RNA was prepared from cells using RNeasy Mini Kit (Qiagen, Valencia, CA). Single-stranded cDNA was synthesized from ~1 μg of total RNA using random hexamers and SuperScript reverse transcription (RT) (Invitrogen) according to the manufacturer's protocols, followed by polymerase chain reaction (PCR) amplification with gene-specific primers using Biolase DNA polymerase (Bioline). Primers, annealing temperatures and product sizes are given in supplementary table 1. The cDNA (1 μl) was replaced by sterile nuclease-free water for negative control in each pair of primers, and no significant band was observed in the negative control. The reaction was conducted using the following protocol: initial denaturing of the template for 5 minutes at 94°C followed by 32 repeating cycles of denaturing for 1 minute at 94°C, annealing for 1 minute, extension for 1 minute at 72°C, and a final elongation at 72°C for 7 minutes. The PCR products were separated by a 1% agarose gel electrophoresis and visualized by ethidium bromide staining.

Electrophysiology

Whole-cell voltage-clamp recordings were performed at room temperature. Pipette electrodes (TW120F-6; World Precision Instruments, Sarasota, FL) were fabricated using either a Sutter P-97 horizontal puller or a Narishige PC-10 vertical puller and had final tip resistances of 3–5 MΩ. Membrane currents were measured using a patch-clamp amplifier (Axon 200B, Axon Instruments), sampled and analyzed using a Digidata 1440A interface and a personal computer with Clampex and Clampfit software (Version 10, Axon Instruments). In most experiments, 70–90% series resistance was compensated. All recordings were performed in external solution consisting of (in mM) NaCl 150, KCl 5, $CaCl_2$ 2, $MgCl_2$ 1, HEPES 10, and glucose 10, pH adjusted to 7.4 with Tris-base. The osmolarity of the solutions was adjusted to 310–320 mosM $liter^{-1}$ with sucrose. The internal solution contained (in mM) NaCl 30, KCl 120, $MgCl_2$ 1, $CaCl_2$ 0.5, HEPES 10, EGTA 5, and MgATP 2, pH adjusted to 7.2 with Tris-base. The osmolarity of the solutions was adjusted to 300–310 mosM $liter^{-1}$ with sucrose. For recording Na^+ currents, K^+ in internal solution was replaced with equimolar Cs^+. The inward voltage-gate Na^+ current was identified by their sensitivity to specific blocker Na_V channel blocker, tetrodotoxin (TTX, 1 μM; Ascent Scientific). For recording K^+ currents, 1 μM TTX was added to the perfusing external solution. Current densities (pA/pF) were calculated as peak outward currents divided by the cell capacitance. Spontaneous postsynaptic currents (sPSCs) were recorded from GFP^+ mESC-OPCs in the co-culture. Combined administration of APV (50 μM; Tocris) and CNQX (10 μM; Tocris) were used to block glutamatergic neurotransmission.

Transplantation

All animal experiments were performed following protocols approved by the Animal Care and Use Committee at the University of California, Davis. The *shiverer* mice at 4~6-week old (Jackson Laboratory) were used for transplantation study. Both spiking and non-spiking mESC-OPCs were suspended at a final concentration of 100,000 cells per μl in PBS (Invitrogen). Under surgical anesthesia, *shiverer* mice were placed in a stereotaxic apparatus (David Kopf Instruments) and received 2 μl of cell suspension either injected into the spinal column between T12 and T13 or injected into the brain corpus callosum (anteroposterior: 0.5 mm, lateral: 2 mm, dorsoventral: 2 mm with reference to bregma). For transplantation into the spinal cord, the procedure was performed according to a previous study [15]. Control animals received injections of 2 μl PBS. Starting from one day before surgery, all animals received daily injections of 10 mg/kg cyclosporine (Millipore) for the duration of the study. Two or three weeks after transplantation or control injection, animals were deeply anesthetized and transcardially perfused with 4% paraformaldehyde in 0.1 M PBS, pH 7.4. The spinal cords and brains were removed and post-fixed for 2 h in the same fixative, and then placed in 30% sucrose in PBS at 4°C for 24 h. Transverse sections were cut at 16-μm thickness using a cryostat, then processed for immunohistochemistry and viewed under a Nikon Eclipse C1 confocal laser-scanning microscope.

Immunostaining and Cell Counting

Cells were cultured on 12-mm glass coverslips (Deckglaser, Germany) and fixed in 4% paraformaldehyde in PBS for 15 min at room temperature. After washing with PBS, cells were permeablized for 10 min in 0.1% Triton X-100, and incubated for 1 h in blocking buffer (5% goat or donkey serum and 1% bovine serum albumin) to reduce nonspecific binding. Cells then were incubated in primary antibodies diluted in blocking buffer at 4°C overnight. Appropriate fluorescence-conjugated secondary antibodies were used for single and double labeling. For staining of NG2 and A2B5 antigens, live cells were incubated with primary antibodies for 15 min, and then fixed in 4% PFA. After permeablization and incubation in blocking buffer as described above, the cells were exposed to appropriate secondary antibodies. For immunostaining on the spinal cord or brain sections of *shiverer* mice, sections were blocked and incubated with the primary antibodies overnight at 4°C, followed by incubation of appropriate fluorescence-conjugated secondary antibodies. All antibodies were tested for cross-activity and nonspecific immunoreactivity.

The primary antibodies used in this study were listed in supplementary table 2. 4′, 6-diamindino-2-phenylindole, dihydrochloride (DAPI, 1:100; Invitrogen) was used to identify the nuclei. Slides or coverslips were mounted with the anti-fade Fluoromount-G medium (Southern Biotechnology). Images were captured using a Nikon Eclipse C1 confocol laser-scanning microscope.

The cells were counted with the ImageJ software (NIH). For cultured cells, at least five fields of each coverslip were chosen randomly and three coverslips in each group were counted. For brain sections, an average of three sections was counted per mouse spanning 160 μm along the antero-posterior aixs.

Transmission Electron Microscopy (TEM)

Mice were perfused and fixed overnight in Karnovsky's fixative (5% glutaraldehyde + 4% formaldehyde in 0.08 M phosphate buffer). The brain samples were post-fixed in 2% osmium tetroxide in 0.1 M cacodylate buffer. Samples were subsequently dehydrated gradually from 50% to absolute ethanol, placed in propylene oxide and then embedded in epon. Semi-thin (1 μm) sections were stained with toluidine blue to aid in orientation of white matter tracts. Ultrathin sections (70 nm) were cut for regions of interest using an

ultramicrotome (Leica). Ultrathin sections were collected on Formva coated single slot copper grids. Ultrathin sections were stained for uranyl acetate and lead citrate and examined in a Philips CM120 Electron Microscope at 80kV. Low magnification images were taken to view the axon distributions, high magnification images were obtained to show the myelin sheath layers for *g*-ratio calculation. Images were acquired via a high resolution CCD camera (Gatan) and processed in DigitalMicrograph (Gatan). Images were imported to Adobe Photoshop for adjusting the brightness and contrast and composing figures.

For quantification of myelinated axons, at least 10 low magnification images (×5000) from three animals (n = 3) were used in control group and groups received spiking and non-spiking mESC-OPCs. Each image covered approximately 180 μm^2 region. All the axon profiles (myelinated and unmyelinated axons) in the region were identified based on the ultrastructural features such as neurofilaments and mitochondria, in most case no synaptic contacts [26]. The percentage of myelinated axons (contain at least 2 myelin sheath layers) were calculated as following: Percentage of myelinated axon = number of myelinated axons / total number of axons × 100%. Quantification of *g*-ratio was carried out from animals received spiking and non-spiking mESC-OPCs. The myelin sheaths were clearly identified in animals received both types of mESC-OPCs. For each group, at least 20 myelinated axon profiles were identified from three animals (n = 3) and photographed at ×17500 – ×20000. Digital photographs showing myelinated axons were imported to Image J (NIH) for *g*-ratio analysis which was calculated by dividing the diameter of the axon by the diameter of the entire myelinated caliber.

Data Analysis

All data represent means ± s.e.m..Student *t* tests were performed to evaluate the statistical significance of difference between two groups. ANOVA followed by Tukey *post hoc* test was performed for multiple comparisons. Values of $p < 0.05$ were considered statistically significant.

Results

Pur- and RA-induced differentiation of GFP-Olig2 mESCs recapitulates the *in vivo* mouse embryonic development and efficiently generates GFP$^+$/Olig2$^+$ OPCs at day 30

In the existing protocols [13, 22, 27] for deriving OPCs from mESCs, the first step usually involves the induction Olig2 expression in the mESC-derived neural progenitor cells, because Olig2 is required for oligodendrocyte development in mice [28]. Previous studies show that treatment of retinoic acid (RA) and Shh efficiently induces neural differentiation of mESCs, which recapitulates *in vivo* mouse embryonic development at the spinal pMN domain that Olig2$^+$ progenitors sequentially generate motoneurons and OPCs at the early and late stages, respectively [13, 27, 29, 30]. In order to examine whether the differentiation process induced by adding RA and purmorphamine (Pur), a small-molecule activator of the Shh signaling pathway [31], recapitulates *in vivo* mouse embryonic development, we induced GFP-Olig2 mESCs differentiation (Fig. 1A) and assessed the composition of the cell populations at the differentiation day 10, 20 and 30. As shown in Fig. 1B and C, the expression of NG2 and another marker for OPCs, A2B5 [32] at day 10 were detected at low percentage (7.9 ± 1.7% and 4.9 ± 0.7% for NG2$^+$ and A2B5$^+$, respectively). To examine the percentage of neurons, the neuronal marker βIII-tubulin and the motoneuron lineage marker HB9 were stained. At day 10, βIII-tubulin and HB9 positive cells were detected at the rate of 12.7 ± 2.0% and 8.2 ± 1.3%, respectively (Fig. 1B and C). At day 20 in culture, the percentage of NG2 and A2B5 positive cells showed a dramatic increase (Fig. 1B and C, 54.0 ± 4.2 % for NG2$^+$ and 40.1 ± 8.3% for A2B5$^+$). However, after 3–4 passages, the percentage of βIII-tubulin and HB9 positive cells decreased at D20 to 0.8 ± 0.5% and 0.6 ± 0.3%,

respectively, suggesting the decreased capability of generating motoneurons from the $Olig2^+$ progenitors at D20. At D30, the percentage of NG2 and A2B5 positive cells reached 81.8 ± 1.3% and 82.8 ± 2.4%, respectively (Fig. 1B and C), and βIII-tubulin and HB9 positive cells were not observed (Fig. 1C). Throughout the differentiation period, no GFAP positive astrocytes were observed (Fig. 1B and C). Thus, despite replacing Shh with Pur, mESC differentiation process recapitulates the mouse embryonic development. Moreover, as shown in Fig. 1A and D, at day 30, 96.4 ± 1.3% of GFP positive cells were NG2 positive, and 94.8 ± 1.5% of NG2 positive cells were GFP positive. Thus, GFP positive cells co-expressed Olig2 and NG2, which are the hallmarks of OPCs [33, 34]. The GFP expression also overlapped with A2B5 (Fig. 1A and D, 97.0 ± 1.3 % of GFP positive cells were A2B5 positive, and 88.3 ± 4.0 % of A2B5 positive cells were GFP positive). Therefore, using this differentiation protocol, we could obtain OPCs from GFP-Olig2 mESCs with a high efficiency in 30 days. We also double-stained cells at day 10 and 20 for Olig2 and GFP, and found that about 98% of Olig2 expression co-localized with GFP, indicating that GFP fluorescence reliably marked Olig2 expression in this paradigm (Supplementary Fig. 1).

GFP^+ mESC-OPCs differentiate into oligodendrocytes but show different electrophysiological properties from brain-derived OPCs

We next purified mESC-OPCs using FACS based on GFP fluorescence. The FACS analysis showed the percentage of GFP^+ cells increased from 49.1 ± 4.0% at day 10 to 80.3 ± 1.3% at day 30 (Fig 2 A and B, $n = 4$, $p < 0.001$). The purified day 30 GFP^+ mESC-OPCs could be expanded in the OPC medium and could be subjected to the frozen/thaw cycles without losing their capability of proliferation and maturation. Unless otherwise mentioned, the FACS-purified day 30 mESC-OPCs within passage 1 to 6 were used in the following experiments. As shown in Fig. 2C, the purified day 30 mESC-OPCs matured into $O4^+$ and MBP^+ oligodendrocytes when cultured in the presence of thyroid hormone T3, which promotes OPCs differentiation into oligodendrocytes [35]. The inactivating inward currents, which resembled the I_{Kir} were also detected in the GFP^+ cells cultured in the presence of T3, but not in the bipolar mESC-OPCs (supplementary Fig. 2B). These properties thus showed that the mESC-OPCs were capable of differentiating to mature oligodendrocytes *in vitro*.

To further characterize the properties of mESC-OPCs, we compared the electrophysiological properties of the mESC-OPCs with those of primary cultures of mouse brain OPCs. We recorded 96 GFP^+ mESC-OPCs by whole-cell patch-clamp recordings. The mESC-OPCs had an average capacitance of 9.7 ± 0.8 pF and particularly a high resistance of 1.1 ± 0.1 GΩ, a characteristic of OPCs [6]. Next, we tried to record inward currents from mESC-OPCs using Cs^+ internal solution which could completely block the outward potassium currents. Unexpectedly, no inward currents could be recorded from any mESC-OPCs, while inward I_{Na} could be observed from cultured brain OPCs and were sensitive to 1 μM TTX (Fig 2D). When held at – 60 mV under current-clamp, no spikes could be stimulated from mESC-OPCs even though the membrane potential was depolarized to 0 mV, while slight spikes were observed from cultured brain OPCs (Fig 2D), which is consistent with previous recordings from rodent OPCs in culture [4]. We also recorded the mESC-OPCs cultured for 50 days, and no I_{Na} was observed, suggesting that the lack of I_{Na} was unlikely due to a development delay in *in vitro* culture. The same results were also observed from the mESC-OPCs generated by adding Shh peptide instead of Pur during the differentiation process, suggesting these differences were not resulted from replacing Shh peptide with Pur. To compare the outward potassium currents in mESC-OPCs and cultured brain OPCs, we then recorded the whole-cell voltage-gated ionic currents in the presence of 1 μM TTX with a pre-pulse to − 80 mV. The delayed rectifier potassium current (I_{KD}) were isolated by using a pre-pulse to + 20 mV, which inactivated the currents carried by outward inactivating A-type potassium current (I_{KA}). To reveal I_{KA}, the currents elicited following a pre-pulse to + 20

mV were digitally subtracted from those elicited following pre-pulse to − 80 mV. Both I_{KD} and I_{KA} components were detected in mESC-OPCs and cultured brain OPC (Fig. 2E). I-V relationships of I_{KD} and I_{KA} were shown in Fig. 2F and G, respectively. Notably, the current densities of I_{KD} and I_{KA} were much larger in mESC-OPCs than those in the cultured brain OPCs.

Non-spiking mESC-OPCs acquire spiking properties after ectopic expression of $Na_V1.2$ subunit

To explore whether Na_V subunit transcripts could be detected in the mESC-OPCs, we performed PCR on cells at differentiation day 10 and FACS-purified day 30 mESC-OPCs. As shown in Fig 3A, consistent with the immunostaining results showing that neurons existed at day 10 (Fig. 1A), multiple Na_V transcripts were identified from day 10 unpurified cells, such as transcripts that encode CNS (SCN2A, SCN3A) and dorsal root ganglion (SCN10A, SCN11A) Na_V α subunits. Some other transcripts encoding skeletal (SCN4A) and cardiac (SCN5A, SCN7A) Na_V α subunits were also detected. None of β subunit transcripts were detected in day 10 cells. In day 30 purified GFP^+ mESC-OPCs, of all sodium channel genes (10 α and 4 β subunits) studied, only the SCN1B transcripts, which encode the Na_V β1 auxiliary subunit, were detected. Consistent with the immunostaining results (Fig. 1A and supplementary Fig. 1), the Olig2 transcripts were detectable at day 10 but strongly expressed at day 30, and the NG2 transcripts were nearly undetectable at day 10 but highly expressed at day 30. Thus, due to the lack of expression of pore-forming Na_V α subunit transcripts, the D30 mESC-OPCs did not show any detectable I_{Na} (Fig. 2D).

We next sought to generate functional I_{Na} in the day 30 mESC-OPCs. SCN2A gene, which encodes $Na_V1.2$ α subunit, is expressed in the CNS OPCs and is the most significantly changed sodium channel during the maturation of OPCs to pre-oligodendrocytes [5, 36]. Thus, we transduced the mESC-OPCs with baculovirus carrying the gene SCN2A. As shown in Fig 3B, the expression of SCN2A gene transcript was detected from 1 to 3 days after viral infection, and then gradually deceased over time in culture and was undetectable at 8 days after viral infection. The high efficiency of viral infection was demonstrated by the observation that the majority of the GFP^+ cells were positive for $Na_V1.2$ staining (Fig. 3C). The GFP^+ cells remained positive for A2B5, indicating their unchanged identity as OPCs (Fig. 3C). Patch-clamp recordings performed from 1 to 3 days after viral infection also showed that 94.1% of mESC-OPCs (16 of 17) expressed inward currents and all of the cells (17 of 17) continued to express outward potassium currents (Fig. 3D). The sensitivity to TTX and I-V relationship of the inward currents indicated their nature of I_{Na} (Fig 3D and E). Under current-clamp recording, when the membrane potentials were held at − 60 mV, these transduced cells generated single spikes that grew in size as the depolarization was gradually increased (Fig. 3F). When held at −100 mV, the spike threshold was more negative and spike magnitudes were increased. Some of the cells (17.6%, 3 of 17) held at −100 mV fired all-or-none action potentials (Fig. 3F).

We next attempted to search for extracellular factors including growth factors and morphogens that have been implicated in OPC differentiation conditions to see which would induce expression of Nav in the cells and drive the mESC-OPCs to electrical activity. Thus, we examined whether different culture conditions could trigger and maintain the expression of I_{Na} in the mESC-OPCs. First, Pur, FGF2 and PDGF were routinely added into the OPC culture medium. However, these mESC-OPCs did not show functional I_{Na}, indicating that long-term culture in the presence of the morphogen Shh agonist Pur and the growth factors FGF2 and PDGF did not promote I_{Na} expression. As neuregulins critically regulate the survival, mitosis, migration and differentiation of oligodendrocyte lineage cells [37–39], we next tested the addition of heregulin, a key member of neuregulin-1 family, to the OPC culture medium and cultured the mESC-OPCs for 7–10 days. However, no I_{Na} was detected

in these mESC-OPCs. In addition, as previous studies have shown that the interaction between axonal laminin and oligodendroglial integrin contributes importantly to the formation of myelin sheath [40], and laminin modulates the expression of sodium channel-mediated currents in CNS progenitor cells [41] and epithelial cells [42], we then cultured the mESC-OPCs on laminin-coated coverslips in the OPC medium containing laminin. Interestingly, after 7–10 days, 7.7% of the mESC-OPCs (1 in 13) expressed TTX-sensitive I_{Na} (Fig. 3G). Although the amplitude of I_{Na} was small, slight spikes were observed (Fig. 3H), indicating that laminin was capable of inducing electrical activity in mECS-OPCs, but did not work robustly.

Spiking mESC-OPCs receive synaptic input from neurons and show superior capability of maturation into oligodendrocytes *in vitro*

Spiking and non-spiking OPCs have been identified in the rodent brain. However, the functional differences between these two subtypes of OPCs are largely unclear. To address this question, we used the mESC-OPCs with distinct electrophysiological properties, i.e. spiking and non-spiking mESC-OPCs, to perform comparison studies. To achieve optimum comparisons, we used the spiking mESC-OPCs generated by viral transduction of $Na_V1.2$ α subunit in these experiments. We first co-cultured the spiking and non-spiking mESC-OPCs with primary mouse hippocampal neurons. Two days after co-culture, we patch-clamped both mESC-OPCs identified by GFP fluorescence (Fig. 4A). We observed that about 40% (6 out 15) of the spiking mESC-OPCs showed I_{Na} after 2 days in co-culture and no I_{Na} was detected in any non-spiking mESC-OPCs. We also found that no spontaneous postsynaptic currents (sPSCs) were detected in any non-spiking mESC-OPCs co-cultured with the neurons. Interestingly, sPSCs were recorded from some of the spiking mESC-OPCs (13.3%, 2 out of 15) and the sPSCs were completely blocked by APV and CNQX (Fig. 4B), indicating that the sPSCs were glutamatergic excitatory neurotransmissions. This observation is consistent with and in support of a previous report showing that spiking OPCs, but not non-spiking OPCs, receive synaptic input from axons [10]. We further asked whether the expression of I_{Na} in mESC-OPCs could affect their maturation in the co-culture. Ten days after co-culture, we triple stained the cells with GFP, MBP and neuronal marker MAP2. As shown in Fig. 4C, there were many $MAP2^+$ neurons in the culture and the presence of neurons largely promoted the maturation of both spiking and non-spiking mESC-OPCs into MBP^+/GFP^+ oligodendrocytes that were readily distinguished from endogenous MBP^+ but GFP^- (negative) oligodendrocytes in the primary culture. Quantitative analysis showed that the percentage of MBP^+/GFP^+ cells over total GFP^+ cells was significantly higher in the co-culture with spiking mESC-OPCs than that in the co-culture with non-spiking mESC-OPCs (Fig. 4C and D, 10.4 ± 3.9% and 23.4 ± 9.6% for co-culture with non-spiking and spiking mESC-OPCs, respectively; $p < 0.05$, $n = 4$). We also examined the co-culture of neurons with mESC-OPCs infected with control virus. Similar results to mESC-OPCs without viral infection were obtained, indicating that the observation was not resulted from the viral infection.

Spiking mESC-OPCs show better capacity of maturation and myelination after transplantation into the *shiverer* mouse

The *shiverer* mouse is an autosomal recessive mutant that lacks a functional gene for MBP, an essential component of myelin required for formation of compact mature myelin, and thus displays abnormal and poor CNS myelination [43–45]. The *shiverer* mice are widely employed to study the myelinating capability of exogenously grafted cells [46]. To further examine the capacity of maturation and myelination of the non-spiking and spiking mESC-OPCs *in vivo*, we first transplanted the mESC-OPCs into the dorsal column spinal cord of *shiverer* mice. Three weeks after transplantation, the control animals without receiving any grafted cells and animals received transplantation of mESCs-OPCs were euthanized and

processed for immunostaining. No tumor formation or overgrowth of the transplanted cells was observed. As shown in Fig. 5A, the majority of the GFP^+ cells were found in proximity to the injection site. We noticed that although many transplanted spiking and non-spiking mESC-OPCs matured into MBP^+ oligodendrocytes, the transplanted cells remained round-shaped and did not form long and "railway track-like" myelin segments [47] (Fig. 5A), similar to the results obtained by a recent report after transplanting mESC-OPCs into a rat spinal cord injury model [48]. As shown in Fig. 5C, there were some GFP^+ cells from both cell transplantation groups showing the OPC marker NG2 (Fig. 5B). We also found that very few GFP^+ cells (< 1%) overlapped with GFAP staining, and there was no significant difference between non-spiking and spiking mESC-OPC groups. Notably, the percentage of GFP^+ cells that were MBP^+ in the spiking mESC-OPC group was significantly higher than that in the non-spiking mESC-OPC group (Fig. 5C, 88.1 ± 2.5% and 77.2 ± 3.3% for spiking and non-spiking mESC-OPC groups, respectively, $p < 0.05$, n = 6 for each group), indicating that spiking mESC-OPCs had better capability of maturing into MBP-expressing oligodendrocytes than the non-spiking OPCs *in vivo*.

To promote formation of myelin segments and further compare the capability of myelination between spiking and non-spiking mESC-OPCs, we transplanted the mESC-OPCs into the corpus callosum where the bundles of axon fibers are highly enriched. Two weeks after transplantation, the animals were euthanized and processed for immunostaining. We found that only some short myelin segments were observed from the animals received non-spiking mESC-OPCs (Fig. 6A), while long and "railway track-like" myelin segments were observed from the animals received spiking mESC-OPCs (Fig. 6B). We also noticed that the MBP^+ myelin segments did not co-labeled with GFP staining but the cell bodies did weakly express GFP, which could be due to down-regulation of Olig2 expression as the mESC-OPCs initiate the myelination program [49]. Next, we further examined the myelination from control animals and animals received spiking or non-spiking mESC-OPCs with transmission electron microscopy (TEM). As shown in Fig. 6B, only the axons with loose wraps of myelin were seen in the control PBS group. The axons with compact myelin wraps were found in both spiking and non-spiking mESC-OPC groups (Fig. 6C and D). Quantitative analysis showed that the percentage of myelinated axons in 180 μm^2 was significantly higher in spiking and non-spiking mESC-OPC groups than that in control group (Fig 6F, 14.1 ± 4.3%, 57.6 ± 8.1% and 48.7 ± 4.3%, for control, spiking and non-spiking mESC-OPC groups; $p < 0.05$, n = 3 for each group). There was no significant difference in the percentage between spiking and non-spiking mESC-OPC groups, although the mean percentage of spiking group was slightly higher that of non-spiking mESC-OPC group. Importantly, we found that the *g*-ratio of spiking mESC-OPC group was significantly lower than that of non-spiking mESC-OPC group (Fig. 6G, 0.80 ± 0.04 and 0.85 ± 0.03 for spiking and non-spiking mESC-OPC groups, respectively; $p < 0.05$, n = 3 for each group), indicating that the spiking mESC-OPCs had superior capability of myelination over non-spiking mESC-OPCs *in vivo*.

Discussion

In the present study, we showed that OPC differentiation of mESCs induced by small molecules RA and Pur recapitulated mouse embryonic development. However, electrophysiologically, unlike brain OPCs, the mESC-OPCs showed a lack of I_{Na} expression and were incapable of generating spikes upon stimulation. By generating the spiking and non-spiking mESC-OPCs, we revealed a novel function of Na_V of OPCs in their maturation and myelination both *in vitro* and *in vivo*.

Using the current small molecule-based protocol, we found that βIII-tubulin$^+$ and $HB9^+$ cells were detected at D10, and over 80% of the cells expressed OPCs markers NG2 and A2B5 at

D30. This RA- and Pur-induced differentiation from GFP-Olig2 mESCs thus retains the timing observed in embryonic development, and the GFP^+ mESC-OPCs provide an enriched source for studying OPC properties. Compared to previous studies on rodent brain OPCs, the mESC-OPCs obtained in the present study showed both similarities and differences. Similar to brain OPCs, mESC-OPCs terminally differentiated into mature oligodendrocytes. However, under the identical culture condition, we noticed that mESC-OPCs were less efficient in generating mature oligodendrocytes than brain OPCs. Electrophysiologically, similar to brain OPCs, high input resistance and two types of potassium currents, I_{KD} and I_{KA}, were observed in mESC-OPCs. Constistent with previous studies [4–6, 9, 10, 50–53], we observed that brain OPCs express Na_V channels. However, none of the mESC-OPCs showed I_{Na}, and the transcripts of pore-forming Na_V α subunits were undetectable by PCR.

The roles of Na_V channels of OPCs are largely unclear, but studies have suggested their importance in OPC functions. Activation of sodium channels on OPCs contributes to the resting membrane potential of OPCs [8] that might affect the proliferation of OPCs [54], and is required for GABA-induced migration of OPCs [55]. Strikingly, recent studies [10, 53] show that a subset of brain OPCs can fire Na_V channel-mediated action potentials. Neuronal action potentials are known to promote myelination [56, 57]. However, whether the electrical activities of OPCs could also contribute to the myelination is unclear. In the current study, we did not observe significant difference in resting membrane potential and proliferation between spiking and non-spiking mESC-OPCs. Interestingly, we found that despite the lack of pore-forming Na_V α subunits, the mESC-OPCs express the β1 subunit that is known to regulate the level of Na_V channel expression at the plasma membrane, and function as a cell adhesion molecule to interact with extracellular matrix components [58–61]. Therefore, we ectopically expressed $Na_V1.2$ α subunit in the mESC-OPCs by viral infection. The silent non-spiking mESC-OPCs acquired spiking property after the viral infection. Furthermore, by using a co-culture system, we observed that, the spiking, but not non-spiking mESC-OPCs received synaptic input from neurons and showed superior capability of maturing into MBP^+ oligodendrocytes, compared to non-spiking mESC-OPCs. After transplantation into the *shiverer* mice, both spiking and non-spiking mESC-OPCs can wrap the axon and form multi-layer compact myelin, suggesting that functional Na_V channel expression in mESC-OPCs is not required for OPC maturation and myelination. However, the spiking mESC-OPCs showed better capability in myelinating the axons, indicated by the TEM analysis. Mechanistically, we showed that the expression of functional Na_V might be required for introducing the synapse formation between spiking mESC-OPCs and neurons. The synaptic input to spiking OPCs confer them a better sensitivity to the environment [10, 62] and we propose that this synaptic input may further promote their maturation and myelination. To more definitively address the functional roles of Na_V channels of OPCs, it will be necessary to generate conditional knockout mice of Na_V channels in OPCs. In contrast to the previous demonstration that OPCs possess robust spiking properties at either postnatal stages or adulthood [6, 9, 10], a recent study [5] revealed that OPCs in NG2-dsRed transgenic mice only showed tiny Na^+ spikes at the first postnatal week and became completely nonexcitable in adulthood. Further studies are required to clarify the biological functions of Na_V channel of OPCs *in vivo*.

Previous studies have shown that without introducing Na_V channel, OPCs differentiated from PSC produce substantial amount of myelin sheaths in rodents. However, these studies usually injected the PSC-derived OPCs into animals at very early age (embryos, neonate or less than 7-day old animal) [12, 63] or into immune-deficient animals [16] to avoid immune rejection and to achieve substantial myelination. In the current study, we used 4~6-week old *shiverer* mice that had intact immune system. Although immunosuppressant were given daily to animals, the immune rejection might still to a large degree exist, as particularly reflected by the observation that the transplanted cells in the spinal cord remained round

shape and did not form “railway track-like” myelin sheets, similar to the results obtained by a recent report on transplanting the same mESC-OPCs into a rat spinal cord injury model [48]. Therefore, there is much potential that could be developed to promote maturation and myelination of graft PSC-derived OPCs in a system with intact immune reaction. Here, we demonstrated that Na_V channel that afforded the cells spiking properties might be one of such factors that could improve the myelinating potential of grafted OPCs. In the future, it would be interesting to expand upon this study to investigate the electrophysiological properties of human PSC-derived OPCs and to improve the myelination capacity of human OPC after transplantation. In this study, we found that, although not working robustly, laminin might help promote the expression of I_{Na} in the ESC-OPCs. It would be interesting to more exhaustively search for factors that can robustly trigger and maintain Na_V expression in ESC-OPCs, which would help develop optimal differentiation conditions for deriving functional spiking OPCs from human PSCs in the future.

Conclusions

We have characterized electrophysiological profiles of mESC-OPCs in comparison with brain-derived OPCs. Our results show that, while primary OPCs have outward potassium currents including I_{KD} and $I_{KA,}$ and TTX-sensitive inward I_{Na}, only outward potassium currents are detected in mESC-OPCs. We further demonstrate that spiking properties of mESC-OPCs can be restored, and functional maturation and myelination capability of these cells can be enhanced *in vivo* by ectopic expression of the Na_V α subunit. Our functional characterization of mESC-OPCs and their differentiation capacity provides new insights into the mechanisms of OPC differentiation and future PSC-based therapeutic applications.

Supplementary Material

Refer to Web version on PubMed Central for supplementary material.

Acknowledgments

This work was in part supported by grants from National Institutes of Health (R01NS061983 and R01ES015988 to W. D.), the National Multiple Sclerosis Society (to W. D.), and Shriners Hospitals for Children (to W. D.). P. J. is a recipient of a postdoctoral fellowship from Shriners Hospitals for Children. C. C. is supported by a postdoctoral fellowship from California Institute for Regenerative Medicine.

References

1. Nishiyama A, Lin XH, Giese N, et al. Co-localization of NG2 proteoglycan and PDGF alpha-receptor on O2A progenitor cells in the developing rat brain. J Neurosci Res. 1996; 43:299–314. [PubMed: 8714519]
2. Kang SH, Fukaya M, Yang JK, et al. NG2+ CNS glial progenitors remain committed to the oligodendrocyte lineage in postnatal life and following neurodegeneration. Neuron. 2010; 68:668–681. [PubMed: 21092857]
3. Sontheimer H, Trotter J, Schachner M, et al. Channel expression correlates with differentiation stage during the development of oligodendrocytes from their precursor cells in culture. Neuron. 1989; 2:1135–1145. [PubMed: 2560386]
4. Barres BA, Koroshetz WJ, Swartz KJ, et al. Ion channel expression by white matter glia: the O-2A glial progenitor cell. Neuron. 1990; 4:507–524. [PubMed: 1691005]
5. De Biase LM, Nishiyama A, Bergles DE. Excitability and synaptic communication within the oligodendrocyte lineage. The Journal of neuroscience : the official journal of the Society for Neuroscience. 2010; 30:3600–3611. [PubMed: 20219994]
6. Chittajallu R, Aguirre A, Gallo V. NG2-positive cells in the mouse white and grey matter display distinct physiological properties. J Physiol. 2004; 561:109–122. [PubMed: 15358811]

7. Sontheimer H, Kettenmann H. Heterogeneity of potassium currents in cultured oligodendrocytes. Glia. 1988; 1:415–420. [PubMed: 2976401]
8. Xie M, Lynch DT, Schools GP, et al. Sodium channel currents in rat hippocampal NG2 glia: characterization and contribution to resting membrane potential. Neuroscience. 2007; 150:853–862. [PubMed: 17981402]
9. Ge WP, Yang XJ, Zhang Z, et al. Long-term potentiation of neuron-glia synapses mediated by Ca2+-permeable AMPA receptors. Science. 2006; 312:1533–1537. [PubMed: 16763153]
10. Karadottir R, Hamilton NB, Bakiri Y, et al. Spiking and nonspiking classes of oligodendrocyte precursor glia in CNS white matter. Nat Neurosci. 2008; 11:450–456. [PubMed: 18311136]
11. Clarke LE, Young KM, Hamilton NB, et al. Properties and fate of oligodendrocyte progenitor cells in the corpus callosum, motor cortex, and piriform cortex of the mouse. The Journal of neuroscience : the official journal of the Society for Neuroscience. 2012; 32:8173–8185. [PubMed: 22699898]
12. Brustle O, Jones KN, Learish RD, et al. Embryonic stem cell-derived glial precursors: a source of myelinating transplants. Science. 1999; 285:754–756. [PubMed: 10427001]
13. Shin S, Xue H, Mattson MP, et al. Stage-dependent Olig2 expression in motor neurons and oligodendrocytes differentiated from embryonic stem cells. Stem Cells Dev. 2007; 16:131–141. [PubMed: 17348811]
14. Hu BY, Du ZW, Zhang SC. Differentiation of human oligodendrocytes from pluripotent stem cells. Nat Protoc. 2009; 4:1614–1622. [PubMed: 19834476]
15. Nistor GI, Totoiu MO, Haque N, et al. Human embryonic stem cells differentiate into oligodendrocytes in high purity and myelinate after spinal cord transplantation. Glia. 2005; 49:385–396. [PubMed: 15538751]
16. Wang S, Bates J, Li X, et al. Human iPSC-derived oligodendrocyte progenitor cells can myelinate and rescue a mouse model of congenital hypomyelination. Cell stem cell. 2013; 12:252–264. [PubMed: 23395447]
17. Bunge RP, Bunge MB, Rish. Electron microscopic study of demyelination in an experimentally induced lesion in adult cat spinal cord. J Biophys Biochem Cytol. 1960; 7:685–696. [PubMed: 13805917]
18. Bareyre FM. Neuronal repair and replacement in spinal cord injury. J Neurol Sci. 2008; 265:63–72. [PubMed: 17568612]
19. McFarland HF, Martin R. Multiple sclerosis: a complicated picture of autoimmunity. Nat Immunol. 2007; 8:913–919. [PubMed: 17712344]
20. Xian HQ, McNichols E, St Clair A, et al. A subset of ES-cell-derived neural cells marked by gene targeting. Stem Cells. 2003; 21:41–49. [PubMed: 12529550]
21. Jiang P, Selvaraj V, Deng W. Differentiation of embryonic stem cells into oligodendrocyte precursors. Journal of visualized experiments : JoVE. 2010
22. Chen C, Daugherty D, Jiang P, et al. Oligodendrocyte progenitor cells derived from mouse embryonic stem cells give rise to type-1 and type-2 astrocytes in vitro. Neuroscience letters. 2012; 523:180–185. [PubMed: 22781495]
23. Deng W, Rosenberg PA, Volpe JJ, et al. Calcium-permeable AMPA/kainate receptors mediate toxicity and preconditioning by oxygen-glucose deprivation in oligodendrocyte precursors. Proc Natl Acad Sci U S A. 2003; 100:6801–6806. [PubMed: 12743362]
24. Deng W, Wang H, Rosenberg PA, et al. Role of metabotropic glutamate receptors in oligodendrocyte excitotoxicity and oxidative stress. Proc Natl Acad Sci U S A. 2004; 101:7751–7756. [PubMed: 15136737]
25. Deng W, Neve RL, Rosenberg PA, et al. Alpha-amino-3-hydroxy-5-methyl-4-isoxazole propionate receptor subunit composition and cAMP-response element-binding protein regulate oligodendrocyte excitotoxicity. J Biol Chem. 2006; 281:36004–36011. [PubMed: 16990276]
26. Peters, A.; Palay, SL.; Webster, HD. The Fine Structure of the Nervous System. New York: Oxford University Press; 1991.
27. Du ZW, Li XJ, Nguyen GD, et al. Induced expression of Olig2 is sufficient for oligodendrocyte specification but not for motoneuron specification and astrocyte repression. Molecular and cellular neurosciences. 2006; 33:371–380. [PubMed: 17035043]

28. Ligon KL, Fancy SP, Franklin RJ, et al. Olig gene function in CNS development and disease. Glia. 2006; 54:1–10. [PubMed: 16652341]
29. Samanta J, Kessler JA. Interactions between ID and OLIG proteins mediate the inhibitory effects of BMP4 on oligodendroglial differentiation. Development. 2004; 131:4131–4142. [PubMed: 15280210]
30. Billon N, Jolicoeur C, Ying QL, et al. Normal timing of oligodendrocyte development from genetically engineered, lineage-selectable mouse ES cells. J Cell Sci. 2002; 115:3657–3665. [PubMed: 12186951]
31. Sinha S, Chen JK. Purmorphamine activates the Hedgehog pathway by targeting Smoothened. Nat Chem Biol. 2006; 2:29–30. [PubMed: 16408088]
32. Raff MC, Miller RH, Noble M. A glial progenitor cell that develops in vitro into an astrocyte or an oligodendrocyte depending on culture medium. Nature. 1983; 303:390–396. [PubMed: 6304520]
33. Ligon KL, Alberta JA, Kho AT, et al. The oligodendroglial lineage marker OLIG2 is universally expressed in diffuse gliomas. J Neuropathol Exp Neurol. 2004; 63:499–509. [PubMed: 15198128]
34. Ligon KL, Kesari S, Kitada M, et al. Development of NG2 neural progenitor cells requires Olig gene function. Proc Natl Acad Sci U S A. 2006; 103:7853–7858. [PubMed: 16682644]
35. Baas D, Bourbeau D, Sarlieve LL, et al. Oligodendrocyte maturation and progenitor cell proliferation are independently regulated by thyroid hormone. Glia. 1997; 19:324–332. [PubMed: 9097076]
36. Cahoy JD, Emery B, Kaushal A, et al. A transcriptome database for astrocytes, neurons, and oligodendrocytes: a new resource for understanding brain development and function. The Journal of neuroscience : the official journal of the Society for Neuroscience. 2008; 28:264–278. [PubMed: 18171944]
37. Flores AI, Mallon BS, Matsui T, et al. Akt-mediated survival of oligodendrocytes induced by neuregulins. The Journal of neuroscience : the official journal of the Society for Neuroscience. 2000; 20:7622–7630. [PubMed: 11027222]
38. Lemke G. Neuregulins in development. Molecular and cellular neurosciences. 1996; 7:247–262. [PubMed: 8793861]
39. Burden S, Yarden Y. Neuregulins and their receptors: a versatile signaling module in organogenesis and oncogenesis. Neuron. 1997; 18:847–855. [PubMed: 9208852]
40. Buttery PC, ffrench-Constant C. Laminin-2/integrin interactions enhance myelin membrane formation by oligodendrocytes. Molecular and cellular neurosciences. 1999; 14:199–212. [PubMed: 10576890]
41. Feldman DH, Thinschmidt JS, Peel AL, et al. Differentiation of ionic currents in CNS progenitor cells: dependence upon substrate attachment and epidermal growth factor. Exp Neurol. 1996; 140:206–217. [PubMed: 8690063]
42. Yang JZ, Ho AL, Ajonuma LC, et al. Differential effects of Matrigel and its components on functional activity of CFTR and ENaC in mouse endometrial epithelial cells. Cell Biol Int. 2003; 27:543–548. [PubMed: 12842093]
43. Dupouey P, Jacque C, Bourre JM, et al. Immunochemical studies of myelin basic protein in shiverer mouse devoid of major dense line of myelin. Neuroscience letters. 1979; 12:113–118. [PubMed: 88695]
44. Molineaux SM, Engh H, de Ferra F, et al. Recombination within the myelin basic protein gene created the dysmyelinating shiverer mouse mutation. Proc Natl Acad Sci U S A. 1986; 83:7542–7546. [PubMed: 2429310]
45. Sidman RL, Conover CS, Carson JH. Shiverer gene maps near the distal end of chromosome 18 in the house mouse. Cytogenet Cell Genet. 1985; 39:241–245. [PubMed: 2414073]
46. Liu S, Qu Y, Stewart TJ, et al. Embryonic stem cells differentiate into oligodendrocytes and myelinate in culture and after spinal cord transplantation. Proc Natl Acad Sci U S A. 2000; 97:6126–6131. [PubMed: 10823956]
47. McGregor JEWZ, ffrench-Constant C, Donald AM. Microscopy of myelination. Microscopy: Science, Technology, Applications and Education. 2010
48. Sun Y, Xu CC, Li J, et al. Transplantation of oligodendrocyte precursor cells improves locomotion deficits in rats with spinal cord irradiation injury. PloS one. 2013; 8:e57534. [PubMed: 23460872]

49. Gokhan S, Marin-Husstege M, Yung SY, et al. Combinatorial profiles of oligodendrocyte-selective classes of transcriptional regulators differentially modulate myelin basic protein gene expression. The Journal of neuroscience : the official journal of the Society for Neuroscience. 2005; 25:8311–8321. [PubMed: 16148239]
50. Chvatal A, Pastor A, Mauch M, et al. Distinct populations of identified glial cells in the developing rat spinal cord slice: ion channel properties and cell morphology. Eur J Neurosci. 1995; 7:129–142. [PubMed: 7536092]
51. Sontheimer H, Waxman SG. Expression of voltage-activated ion channels by astrocytes and oligodendrocytes in the hippocampal slice. J Neurophysiol. 1993; 70:1863–1873. [PubMed: 7507520]
52. Zhou M, Schools GP, Kimelberg HK. Development of GLAST(+) astrocytes and NG2(+) glia in rat hippocampus CA1: mature astrocytes are electrophysiologically passive. J Neurophysiol. 2006; 95:134–143. [PubMed: 16093329]
53. Ge WP, Zhou W, Luo Q, et al. Dividing glial cells maintain differentiated properties including complex morphology and functional synapses. Proc Natl Acad Sci U S A. 2009; 106:328–333. [PubMed: 19104058]
54. Pardo LA. Voltage-gated potassium channels in cell proliferation. Physiology (Bethesda). 2004; 19:285–292. [PubMed: 15381757]
55. Tong XP, Li XY, Zhou B, et al. Ca(2+) signaling evoked by activation of Na(+) channels and Na(+)/Ca(2+) exchangers is required for GABA-induced NG2 cell migration. J Cell Biol. 2009; 186:113–128. [PubMed: 19596850]
56. Demerens C, Stankoff B, Logak M, et al. Induction of myelination in the central nervous system by electrical activity. Proc Natl Acad Sci U S A. 1996; 93:9887–9892. [PubMed: 8790426]
57. Stevens B, Porta S, Haak LL, et al. Adenosine: a neuron-glial transmitter promoting myelination in the CNS in response to action potentials. Neuron. 2002; 36:855–868. [PubMed: 12467589]
58. Isom LL. Sodium channel beta subunits: anything but auxiliary. Neuroscientist. 2001; 7:42–54. [PubMed: 11486343]
59. Malhotra JD, Koopmann MC, Kazen-Gillespie KA, et al. Structural requirements for interaction of sodium channel beta 1 subunits with ankyrin. J Biol Chem. 2002; 277:26681–26688. [PubMed: 11997395]
60. Yu FH, Catterall WA. Overview of the voltage-gated sodium channel family. Genome Biol. 2003; 4:207. [PubMed: 12620097]
61. Isom LL. The role of sodium channels in cell adhesion. Front Biosci. 2002; 7:12–23. [PubMed: 11779698]
62. Gallo V, Mangin JM, Kukley M, et al. Synapses on NG2-expressing progenitors in the brain: multiple functions? J Physiol. 2008; 586:3767–3781. [PubMed: 18635642]
63. Hu BY, Du ZW, Li XJ, et al. Human oligodendrocytes from embryonic stem cells: conserved SHH signaling networks and divergent FGF effects. Development. 2009; 136:1443–1452. [PubMed: 19363151]

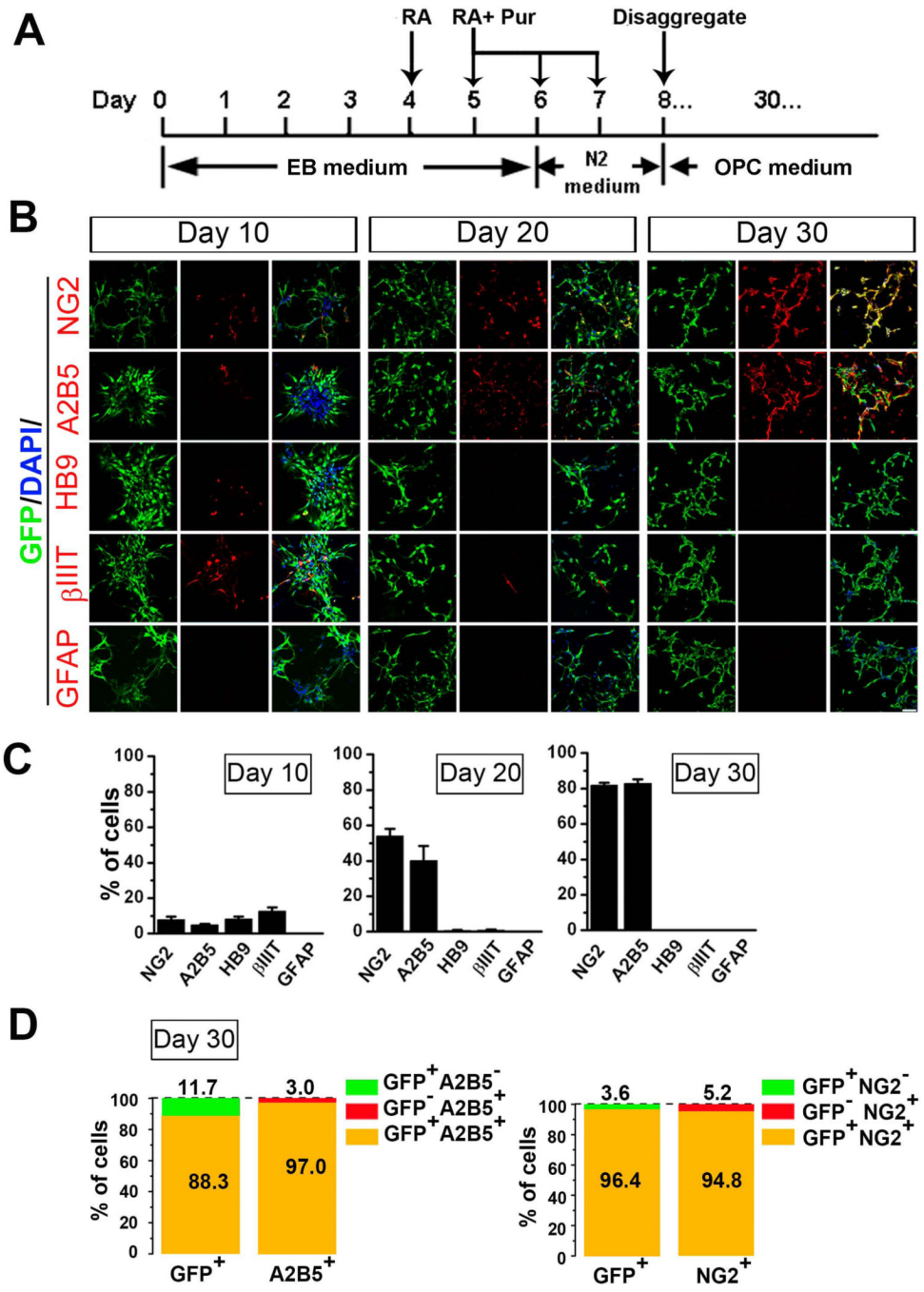

Figure 1. Differentiation of GFP-Olig2 mESCs

(A) Scheme showing the protocol for differentiating mESCs. (B) Panels of representative images showing the immunostaining of NG2, A2B5, HB9, βIII-tubulin (βIIIT), GFAP (all in red) and GFP (green) at differentiation days 10, 20 and 30. Scale bar: 50 μm. Blue, DAPI-stained nuclei. (C) Quantitative analysis showing the percentage of cells expressing NG2, A2B5, HB9, βIII-tubulin and GFAP at the different time points. The percentage of $NG2^+$ and $A2B5^+$ cells showed a dramatic increase from day 10 to day 30. The motoneurons at day 10 were identified by $HB9^+$ and $\beta IIIT^+$ staining. The $HB9^+$ and $\beta IIIT^+$ cells were not observed after several passages to day 30 of differentiation. No $GFAP^+$ cells were observed at any of the three time points. (D) At day 30 of differentiation, $Olig2^+/GFP^+$ cells also

expressed $NG2^+$ or $A2B5^+$, indicating that the majority of $Olig2^+/GFP^+$ cells were OPCs. Abbreviations: mESCs, mouse embryonic stem cells; DAPI, 4′, 6-diamindino-2-phenylindole; OPCs, oligodendrocyte progenitor cells.

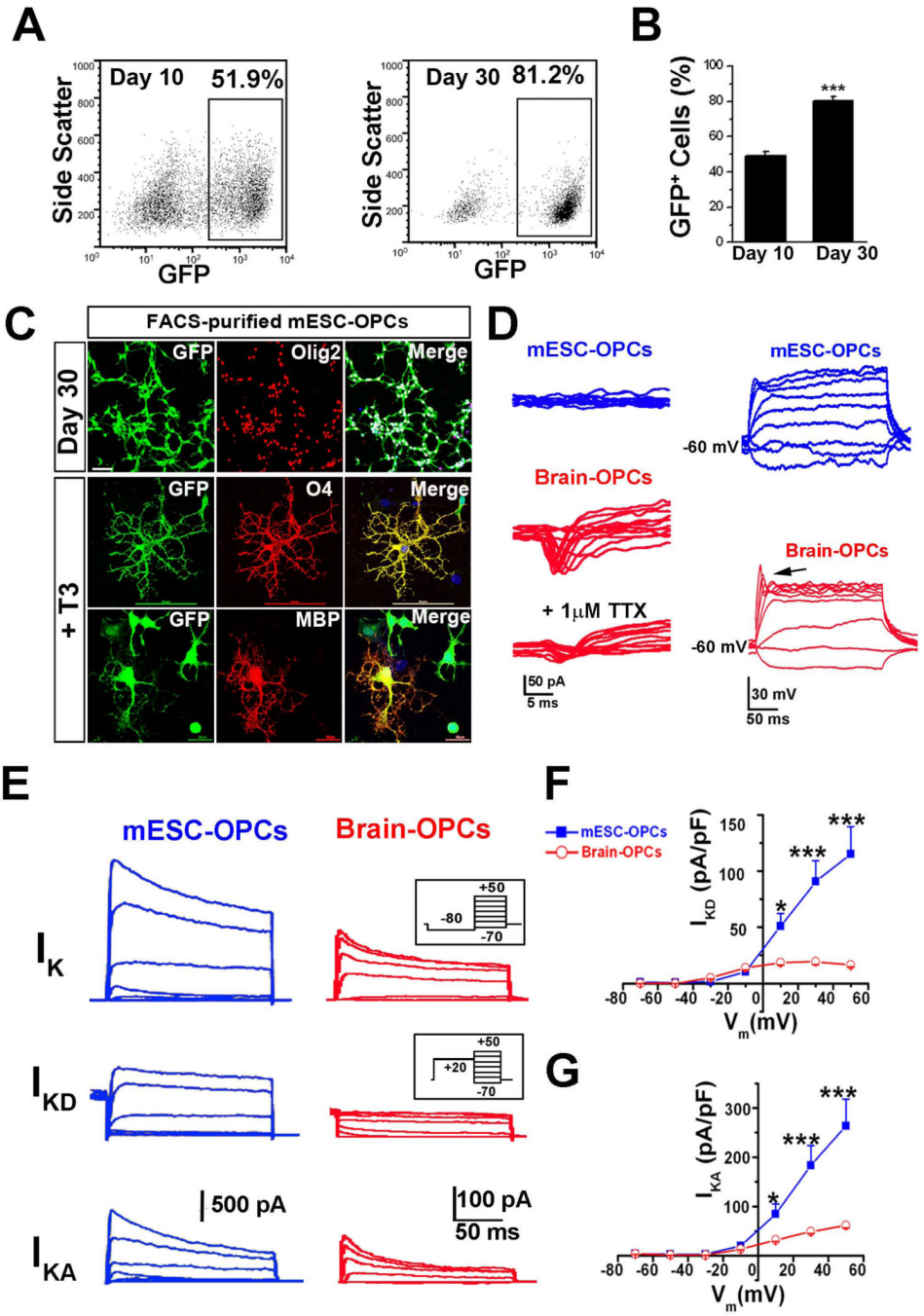

Figure 2. Comparison of electrophysiological properties between GFP$^+$ mESC-OPCs and cultured brain OPCs

(A and B) Representative FACS analysis (A) and quantitative analysis (B) showing that the percentage of Olig2$^+$/GFP$^+$ cells dramatically increased from day 10 to day 30 (n = 4). (C) Representative images showing that the FACS-purified day 30 mESC-OPCs were co-labeled by GFP and Olig2, and matured into O4$^+$ and MBP$^+$ oligodendrocytes in the presence of T3. The scale bars for Olig2 and O4 staining represent 50 μm. The scale bar for MBP staining represents 20 μm. Blue, DAPI-stained nuclei. (D) *Right panels*, representative tracing showing that no I_{Na} was recorded in the mESC-derived OPCs in the presence of Cs^+ internal solution (upper panel), while the TTX-sensitive I_{Na} was present in cultured brain

OPCs (middle and bottom panels). The I_{Na} was elicited by a series of depolarizing voltage steps (from −70 to −50 mV) after a pre-pulse to −100 mV for 100 ms. Similar results were observed from 10 other cells for each group. *Left panels*, representative tracing showing that no spikes were recorded in the mESC-OPCs even when the cell is depolarized to 0 mV (upper panel), while slight spikes were observed in cultured brain OPCs (indicated by the arrow in the lower panel). Current injection: 300 ms, 10 pA steps from −20 to 60 pA. (E) Superimposed current recording in the presence of TTX from a GFP^+ mESC-OPC and a typical cultured brain OPC under voltage clamp at different voltages (200 ms, 20 mV steps from −70 mV to −50 mV) preceded by a pre-pulse conditioning potential of −80 mV, 300 ms (inset, upper panels) or +20 mV, 300 ms (inset, middle panels). With a pre-pulse to −80 mV, overall potassium currents (upper panels) including I_{KA} and sustained outward current I_{KD} was recorded, whereas only I_{KD} (middle panels) could be recorded with a pre-pulse to +20 mV that inactivates I_{KA} component. The traces in bottom panels were of the I_{KA} component and obtained by subtracting the middle panels from the upper panels. (F and G) I-V relationships of the I_{KD} (F) and I_{KA} (G) recorded from mESC-OPCs and cultured brain OPCs (n = 7 for each type of cells). * $p < 0.05$ and *** $p < 0.001$. Data are presented as mean ± s.e.m.. Abbreviations: mESCs, mouse embryonic stem cells; FACS, fluorescence-activated Cell Sorting; T3, 3,3´5´-triido-L-thyronine; OPCs, oligodendrocyte progenitor cells; TTX, tetrodotoxin; I_{Na}, voltage-gated sodium channel-mediated current; I_{KA}, inactivating A-type potassium current; I_{KD}, delayed rectifier potassium current.

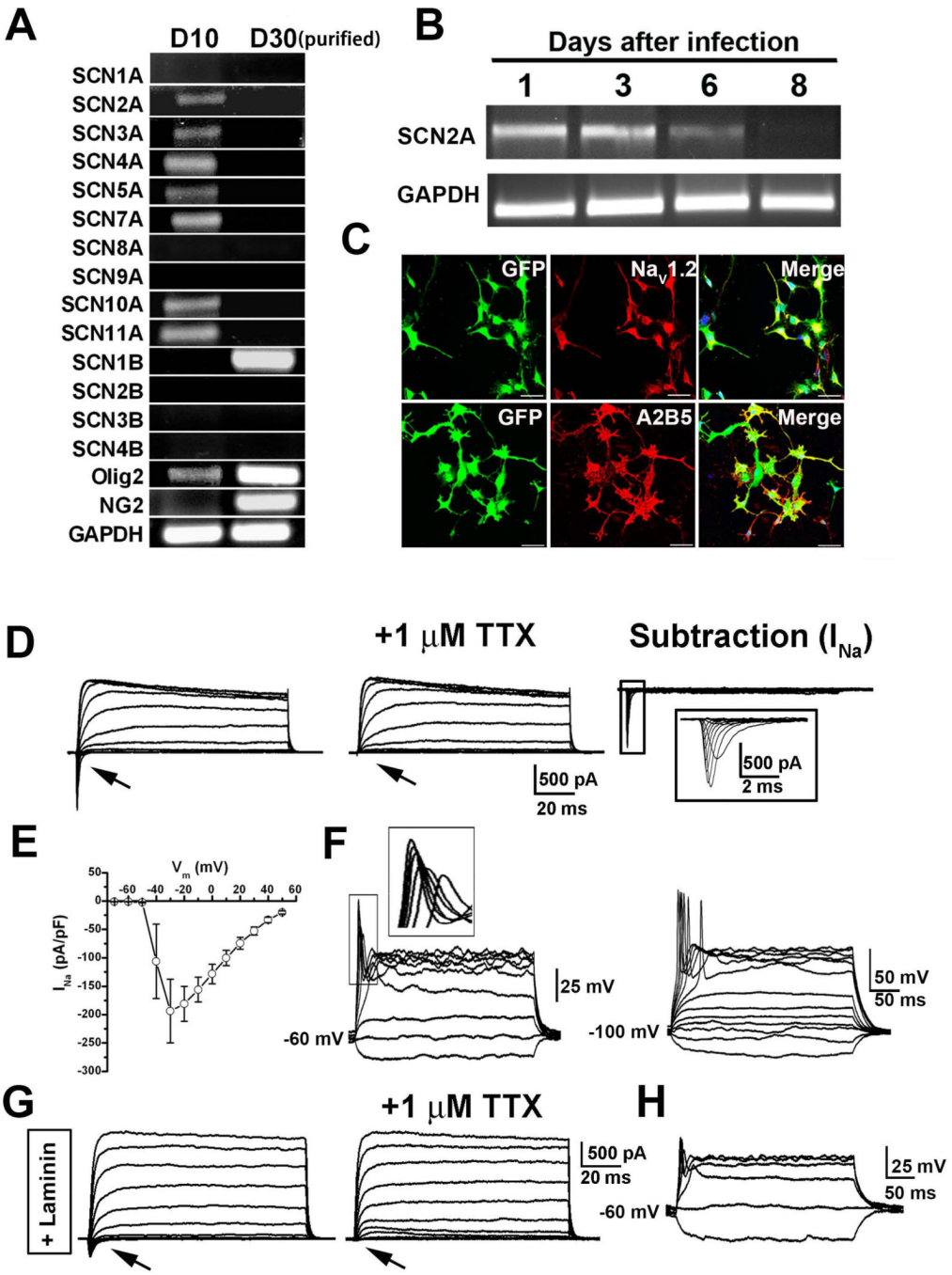

Figure 3. Generation of spiking mESC-OPCs from nonspiking mESC-OPCs

(A) Representative gel image showing the absence of Na_V α subunits and the presence of β1 subunit (SCN1B) in the purified D30 GFP^+ cells. Some of the α subunits were detected in the D10 differentiated cells. In day 10 cells, Olig2 but not NG2 was detectable. In day 30 purified cells, both Olig2 and NG2 were detected. (B) Representative gel image showing that the expression of SCN2A gene transcript was detected one day after infected with baculovirus carrying SCN2A gene, and decreased over time in culture. At 8 days after viral infection, the expression was undetectable. (C) Representative images showing that the mESC-OPCs infected with the baculovirus were positive for $Na_V1.2$ and remained expressing the OPC marker A2B5. Scale bar: 50 μm. Blue, DAPI-stained nuclei. (D)

Representative traces showing the inward TTX-sensitive Na^+ current (indicated by arrows) and outward K^+ current recorded from infected mESC-OPCs. The boxed traces of I_{Na} on the right were enlarged. (E) I-V relationship of I_{Na} recorded from the infected mESC-OPCs (n = 7). (F) *Left*, current-clamp recording showing an example of the transduced mESC-OPC with graded spikes that had greater amplitudes at stronger depolarization (inset), when the membrane potential was held at −60 mV. *Right*, an example of the transduced mESC-OPC firing all-or-none action potentials when the membrane potential was held at −100 mV (current injection, 300 ms, 20 pA steps from −20 to 160 pA). (G) Representative traces showing the TTX-sensitive Na^+ current (indicated by arrows) and outward potassium current recorded from the mESC-OPCs cultured in the presence of laminin. (H) Current-clamp recording showing the slight spikes recorded from the mESC-OPCs cultured in the presence of laminin, when the membrane potential was held at −60 mV (current injection, 300 ms, 20 pA steps from −20 to 80 pA). Abbreviations: mESCs, mouse embryonic stem cells; OPCs, oligodendrocyte progenitor cells; Na_V, voltage-gated sodium channel; DAPI, 4 ´, 6-diamindino-2-phenylindole; TTX, tetrodotoxin.

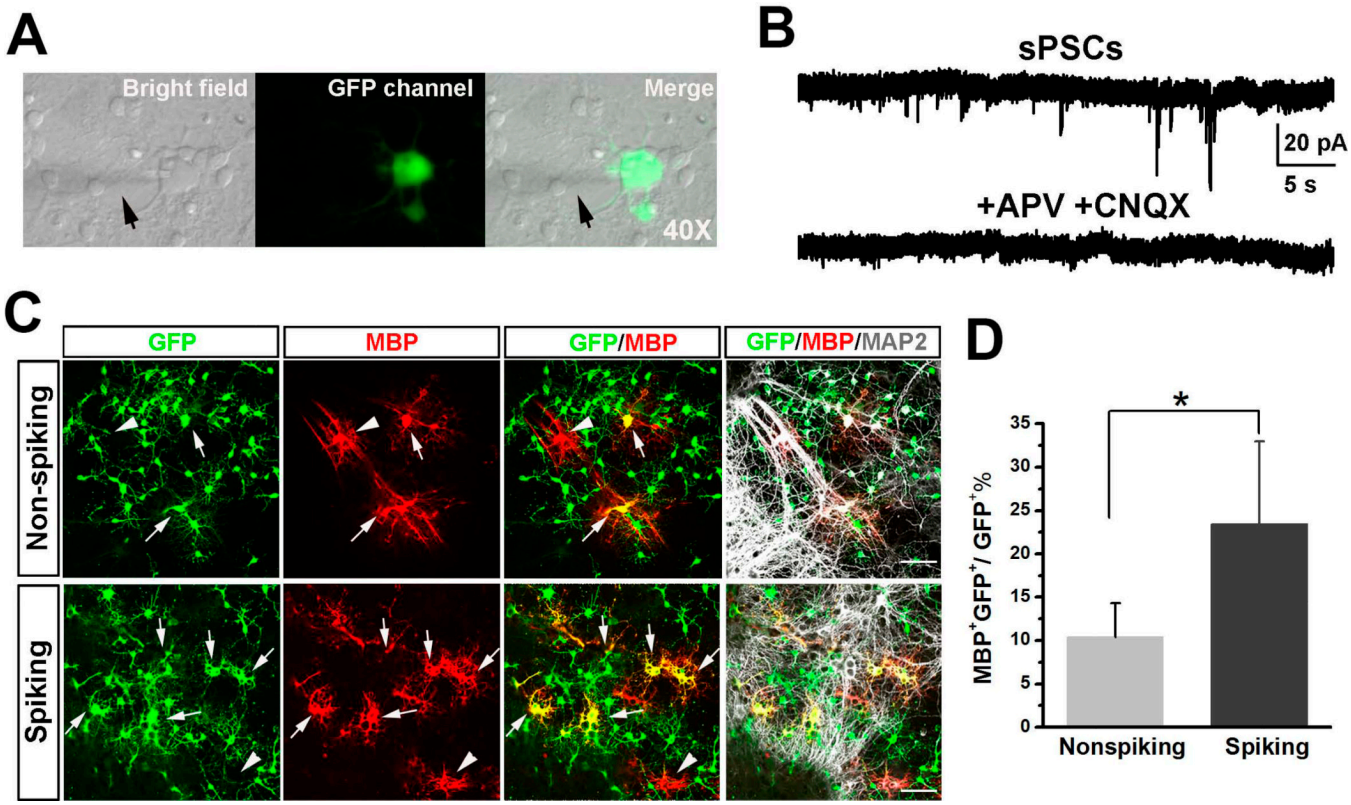

Figure 4. Co-culture of spiking and non-spiking mESC-OPCs with primary mouse hippocampal neurons

(A) Representative phase contrast images of bright filed and GFP channel showing that the mESC-OPCs in the co-culture were identified by GFP fluorescence and patch-clamp recorded. The arrows indicate the recording electrode. (B) Examples of sPSCs recordings from a spiking mESC-OPC and the sPSCs were completely blocked by adding APV and CNQX. (C) Representative images showing that more GFP^+/MBP^+ cells (indicated by arrows) were identified in the co-culture with spiking mESC-OPCs than in the co-culture with non-spiking mESC-OPCs. The arrowheads indicate the GFP^-/MBP^+ endogenous oligodendrocytes from the primary culture. Scale bars represent 50 μm. (D) Quantification of the percentage of MBP^+/GFP^+ cells over total GFP^+ cells in the co-culture (n = 4). * $p < 0.05$. Data are presented as mean ± s.e.m.. Abbreviations: mESCs, mouse embryonic stem cells; OPCs, oligodendrocyte progenitor cells; sPSCs, spontaneous postsynaptic currents; APV, (2R)-amino-5-phosphonopentanoate; CNQX, 6-cyano-7-nitroquinoxaline-2,3-dione.

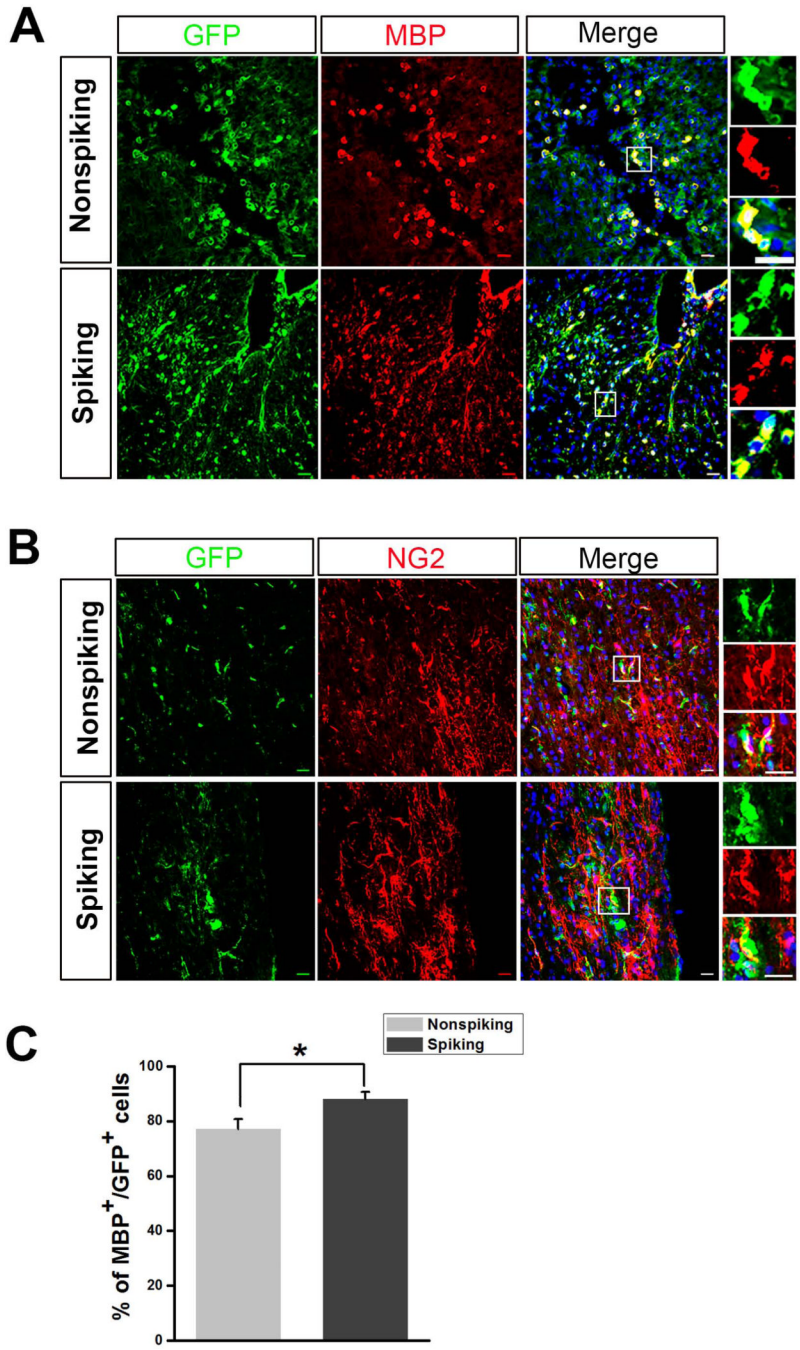

Figure 5. Transplantation of spiking and non-spiking mESC-OPCs into the spinal cord of the *shiverer* mice

(A) Representative images showing that both non-spiking and spiking mESC-OPCs were identified at the injection site as GFP^+ cells (green) and matured into MBP^+ oligodendrocytes (red). Boxed images shown in higher magnification on the right demonstrating that the cells were positive for GFP and MBP. Scale bars represent 20 μm. (B) Representative images showing that some GFP^+ cells were co-labeled by NG2 (red) and GFP (green) staining. Boxed images are shown in higher magnification. Sale bars represent 20 μm. (C) Quantification of the percentage of MBP^+/GFP^+ cells in total GFP^+ cells (n = 6). * $p < 0.05$. Blue, DAPI-stained nuclei. Data are represented as mean ± s.e.m..

Abbreviations: mESCs, mouse embryonic stem cells; OPCs, oligodendrocyte progenitor cells; DAPI, 4′, 6-diamindino-2-phenylindole.

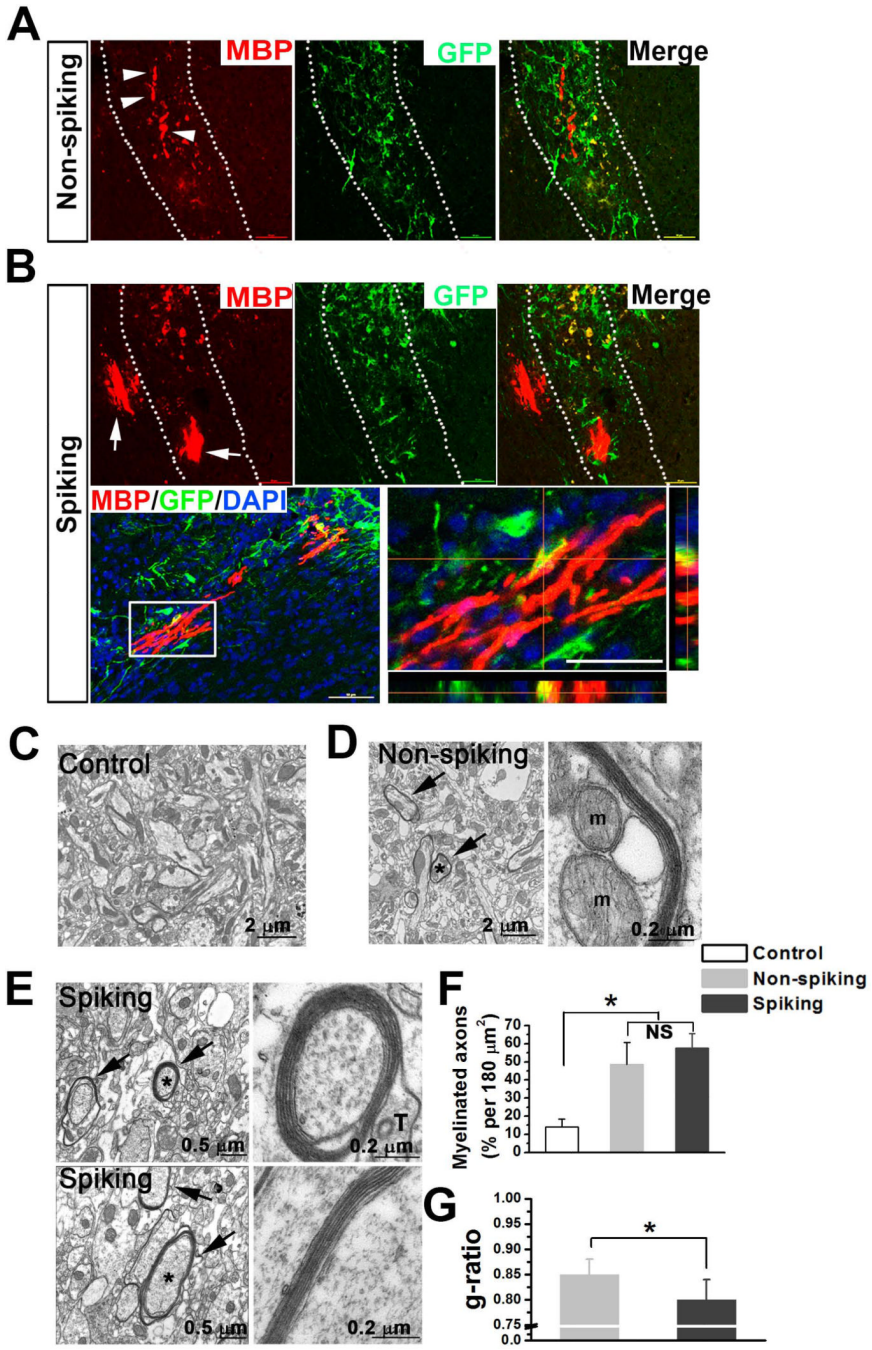

Figure 6. Transplantation of spiking and non-spiking mESC-OPCs into the corpus callosum of the *shiverer* mice

(A and B) Representative images showing the transplanted non-spiking (A) and spiking mESC-OPCs (B) were identified in the corpus callosum (highlighted by dotted lines) by GFP staining (green). Arrowheads in (A) and arrows in (B) indicate the MBP^+ (red) myelin segments formed by the non-spiking and spiking mESC-OPCs, respectively. Lower panels in (B) showing the long and "railway track-like" myelin segments formed by spiking mESC-OPCs. Blue, DAPI-stained nuclei. Note that although the MBP^+ myelin segments did not overlap with GFP staining, the cell body was label by MBP and GFP. (C) Electron micrograph showing that the axons from control *shiverer* animals had no wraps of myelin or

very thin myelin sheath (less than two layers). Scale bar represents 2 μm. (D) Electron micrographs showing the myelination from the animals received non-spiking mESC-OPCs. Arrows in right panel indicate the myelinated axons. One of the myelinated axons (asterisk) showed well preserved wraps of myelin, and a portion of the axon was shown at higher magnification in the right panel. Note that the layers of myelin were clearly seen and two mitochrondria (M) were identified in axoplasm. Scale bars represent 2 μm and 0.2 μm in the left and right panels, respectively. (E) Electron micrographs showing the myelination from the animals received spiking mESC-OPCs. Arrows in right panel indicate the myelinated axons. The axons with asterisk were shown at higher magnification in the right panels. Note that the myelin sheaths were much thicker and a clear external tongue process (T) [26] was also observed. Scale bar represents 0.5 μm and 0.2 μm in the left and right panels, respectively. (F and G) Quantitative analysis showing the percentage of myelinated axons counted in 180 um^2 imaging region for the three groups (n = 3 for each group) (F) and *g*-ratio calculations from spiking and non-spiking groups (n = 3 for each group) (G). * $p < 0.05$. Data are represented as mean ± s.e.m.. Abbreviations: mESCs, mouse embryonic stem cells; OPCs, oligodendrocyte progenitor cells; DAPI, 4′, 6-diamindino-2-phenylindole.